190

A NUMERICAL HYDRODYNAMIC MODEL APPLIED TO TIDAL DYNAMICS IN THE DAMPIER ARCHIPELAGO

DEPARTMENT OF CONSERVATION AND ENVIRONMENT
PERTH WESTERN AUSTRALIA
Bulletin 190 April 1985

A NUMERICAL HYDRODYNAMIC MODEL APPLIED

TO

TIDAL DYNAMICS IN THE DAMPIER ARCHIPELAGO

D.A. MILLS

DAMPIER ARCHIPELAGO MARINE STUDY

DEPARTMENT OF CONSERVATION AND ENVIRONMENT
1 MOUNT STREET
PERTH WESTERN AUSTRALIA 6000

ABSTRACT

This paper introduces a two-dimensional, vertically-integrated,finite-difference, hydrodynamic model which simulates water movements on continental shelves, in nearshore waters, coastal inlets and embayments. The model provides spatial and temporal information on the variations of water level and depth-averaged currents which result from tidal, wind or regional forcing acting on areas of known bathymetry.

The theoretical basis of the model and the stages of its development and testing are outlined.

The model was first applied to investigate the semi-diurnal tides and tidal currents of the Dampier Archipelago and adjacent North-West Shelf. Results obtained from the model are presented, discussed, and shown to compare favourably with tide gauge and current meter data collected in the study area. Predicted surface elevations show an increase in amplitude cross-shelf (shoreward). Simulated tidal currents on the shelf have significant long-shelf components which are driven by a long-shelf gradient of the tidal amplitude. Tidal currents within the Archipelago are primarily influenced by the bathymetry, the local effects of bottom friction, and the nature of the tidal current regime on the shelf. Spatial variations are complex. Peak current speeds in excess of 70 cm s^{-1} are predicted to occur near the western seaward entrances of the Archipelago under mean spring tide conditions. However, tidally-induced residual water flux through the area is low.

Presently the model is being used to estimate residual water fluxes through the Archipelago under combined conditions of tide, wind and regional forcing.

It is planned to extend the model in two ways: to allow for the wetting and drying of inter-tidal banks, and to simulate the transport of materials released to the water from point or diffuse sources.

ISBN 0 7244 6859 5

CONTENTS

FIGURES

TABLES

1. INTRODUCTION

Many characteristics of marine environments are conditioned by the movements of the sea. Nutrients, larvae, detritus, suspended sediments, and pollutants may be transported over large distances by water circulation. Currents exert bottom stresses which may influence the distribution of sea floor sediments and biota. Bottom-generated turbulence associated with rapid flow causes mixing; this may lead to a breakdown of vertical density structure in stratified coastal waters, and possibly to the formation of fronts. The extent of rise and fall of the coastal sea level may be a critical factor in the dynamics of beach and littoral zones.

Modern current meter and tide gauge instruments can collect sets of high quality data over long periods; however the deployment of these instruments is a major logistical exercise and hence measurements are generally restricted to a few locations.

In recent years, with the advent of the digital computer, it has become possible to formulate and solve numerical models of the hydrodynamics of coastal water bodies. This paper describes the development, testing and initial application of a vertically-integrated, two-dimensional, non-linear, finite-difference hydrodynamic model, based on the principles of conservation of mass and momentum. Similar models have been used by other investigators to study tidal and wind-driven water movements in various coastal seas and estuaries (eg Flather and Heaps 1975, Pingree and Maddocks 1977, Fandry 1981, Bode et. al. 1981). Using numerical techniques to solve the conservation equations, the models account for the influences on the water motion of wind and tidal forcing, frictional resistance at the sea bed, effects of the earth's rotation, and the shape of the water body in plan and bathymetry. The numerical solution consists of values of surface elevation and vertically-averaged horizontal components of current velocity, evaluated at regular intervals in (horizontal) space and time.

For the model to function, it must be supplied with water level or current data defined at its open (seaward) boundaries. Realistic simulations of natural coastal water movements rely heavily on the accuracy of the open boundary data input to the model.

Available field data, collected from within the modelled area, may be used for comparison with the model results. Such comparisons are highly desirable; however these interior data are not required to make the model function.

Ideally, a programme of calibration and verification should be carried through to assess the level of predictive capability of the model. Calibration involves the adjustment of model parameters to obtain best agreement between field and modelled results under one set of forcing conditions. If, with the same parameter values, the model is able to simulate observed field behaviour under a second set of known forcing conditions, it is said to have been verified.

When this assessment has been made, the model results may be used to interpret available current meter data in terms of the overall hydrodynamic behaviour of the system. The response of the system to separate forcing effects can be isolated and examined in successive model runs. The model can be forced by sets of conditions not encountered during any field measurement

programme. Furthermore, the basic solution variables of surface elevation and vertically-averaged current velocity can be used to derive other relevant information, such as the residual (time-averaged) drift, the distribution of stress exerted on the sea floor, and areas of rapid frictional dissipation of the kinetic energy of currents, often associated with strong vertical mixing.

Initially, the model has been applied to the coastal waters of the Dampier Archipelago and the adjacent continental shelf waters off the north-west of Western Australia. Results presented here are simulations of mean spring tidal conditions and show good agreement with field measurements. Further applications of the model are presently in progress. These are aimed at providing hydrodynamic information applicable to studies of the sediment dynamics, water quality, and biological productivity of the Dampier Archipelago.

The model has a general capability: it can run with different coastal and bathymetric inputs, and be driven by different wind, tidal and other forcing. Thus the model can be adapted to other coastal areas around Western Australia where required.

2. THEORETICAL FOUNDATION

The model is based on a set of partial differential equations expressing the conservation of fluid mass and momentum. For the flow of a homogeneous sea, driven by water-surface slope and wind stress, and damped by bottom friction, the vertically-averaged forms of these equations are:

equation of mass conservation

$$\frac{\partial \zeta}{\partial t} + \frac{\partial (uH)}{\partial x} + \frac{\partial (vH)}{\partial y} = 0 \quad , \qquad (1)$$

equation of momentum conservation

$$\frac{\partial u}{\partial t} + u\frac{\partial u}{\partial x} + v\frac{\partial u}{\partial y} - fv = -g\frac{\partial \zeta}{\partial x} + \frac{(\tau_{sx} - \tau_{bx})}{\rho H} \quad , \qquad (2)$$

$$\frac{\partial v}{\partial t} + u\frac{\partial v}{\partial x} + v\frac{\partial v}{\partial y} + fu = -g\frac{\partial \zeta}{\partial y} + \frac{(\tau_{sy} - \tau_{by})}{\rho H} \quad , \qquad (3)$$

where the notation used is

t	time
x, y	local horizontal Cartesian co-ordinates
u, v	horizontal velocity components averaged vertically through the water column
h	undisturbed water depth
ζ	sea-surface elevation about the undisturbed surface level

$H = h + \zeta$ total water column depth

$f = 2\Omega\sin\Phi$ Coriolis parameter, where Φ is latitude, and Ω is the angular velocity of the earth's rotation

g acceleration due to gravity

ρ density of sea water

τ_{sx}, τ_{sy} components of wind stress acting on the water surface

τ_{bx}, τ_{by} components of frictional stress applied at the sea bed

The vertically-averaged current components are defined as:

$$u = \frac{1}{H}\int_{-h}^{\zeta} u'dz, \quad v = \frac{1}{H}\int_{-h}^{\zeta} v'dz,$$

where u', v' are components of the horizontal current velocity at depth z.

This formulation of the equations can be made assuming that:

- horizontal seawater density gradients are negligible
- vertical accelerations are negligible and fluid pressures hydrostatic
- horizontal shear stresses are negligible
- atmospheric pressure at the sea surface is uniformly distributed
- vertical velocity profiles are nearly uniform, allowing a simple form of the integrated momentum advection terms
- the region being modelled is of small latitudinal extent, so that variations in the Coriolis parameter may be neglected.

These assumptions and their relevance to natural water bodies have been further discussed in Cheng et al. (1976).

Equation (1) states that changes in total height of a column of water are balanced by nett horizontal water flow into or out of that column. In equations (2) and (3), local time variations of the vertically-averaged velocity components result from nett advection of horizontal momentum, the effect of the earth's rotation, horizontal pressure gradient force caused by the sea surface slope, surface wind stress and frictional bottom stress.

The nett advection of momentum allows flow to adjust smoothly to abrupt spatial changes in the forcing. For example, when an intense, near-shore current passes a sharp headland or promontory, it may be displaced off-shore for some downstream distance. Such effects are generally localised and involve redistribution of momentum, but no change to the total momentum input.

The effect of the earth's rotation is equivalent to a force of magnitude proportional to the current speed, and acting to the left (southern hemisphere) of the current direction.

The surface wind stress field may be specified directly, or derived from a wind vector field at a standard height above sea-level, through application of a quadratic stress law (e.g. Hicks 1972).

In the context of a two-dimensional model, it has been assumed that the bottom stress can be related to the depth-averaged velocity. Modelling practice (e.g. Flather & Heaps 1975, Bode et al. 1981) has shown that a quadratic stress law of the form

$$\tau_{bx} = \rho k u (u^2 + v^2)^{1/2} \quad ,$$

$$\tau_{by} = \rho k v (u^2 + v^2)^{1/2} \quad ,$$

generally yields satisfactory results for a constant or weakly depth-dependent drag coefficient, k. Values of k between 0.0025 and 0.003 have frequently been used. Such an approach is empirical and does not incorporate the more fundamental concepts of turbulent boundary layer drag.

For a region of specified plan form and bathymetry, the vertically-integrated equations of motion are solved in space and time, commencing from a known state, and subject thereafter to prescribed conditions at the boundaries of the region. Any initial disturbance will gradually decay due to the influence of bottom friction, and the motion will become increasingly adjusted to continued forcing applied either directly within the model domain (e.g. wind forcing), or introduced through the boundary conditions (e.g. tidal oscillations). The boundary conditions themselves may be specified as time series of either surface elevations, normal velocity components, or gradients of these quantities normal to the boundaries of the domain.

Several terms in the basic equations involve products of the dependent variables ζ, u, v, or their derivatives. These are known as the non-linear terms. The nett horizontal mass flux terms (equation (1)), the nett momentum advection terms and the quadratic bottom stress terms (equations (2) and (3)) fit into this category. The response of a non-linear model to periodic forcing at a given frequency occurs not only at that same frequency, but at higher harmonic frequencies and also as a steady, non-oscillatory response (see Zimmerman 1978, Pingree and Maddock 1978). Such terms may be of importance when assessing, for example, residual water drift, or the preferred directions of stress applied to the sea bed (Howarth and Pugh 1983).

Given the complex form of most natural water bodies and the range of dynamic effects operating on them it is generally impossible to obtain the appropriate solutions by analytical methods, and use is made of numerical solution techniques.

3. NUMERICAL SCHEME

The numerical solution describing the water movement is obtained with reference to a uniform grid forming an array of cells which covers the region under consideration. Figure 1 shows the positioning of three distinct sets of points on this grid, the definition of variables, and the subscript

reference system used. The velocity component v is defined at points located on x-directed cell boundaries. The velocity component u is defined at points on y-directed cell boundaries. At points co-inciding with cell centres, the water elevation ζ, water depth h, and surface wind stress components τ_{sx} and τ_{sy} are specified. Both land and open sea boundaries are approximated by grid cell walls. This grid system is known as the Arakawa (C) or Richardson lattice (Arakawa 1972).

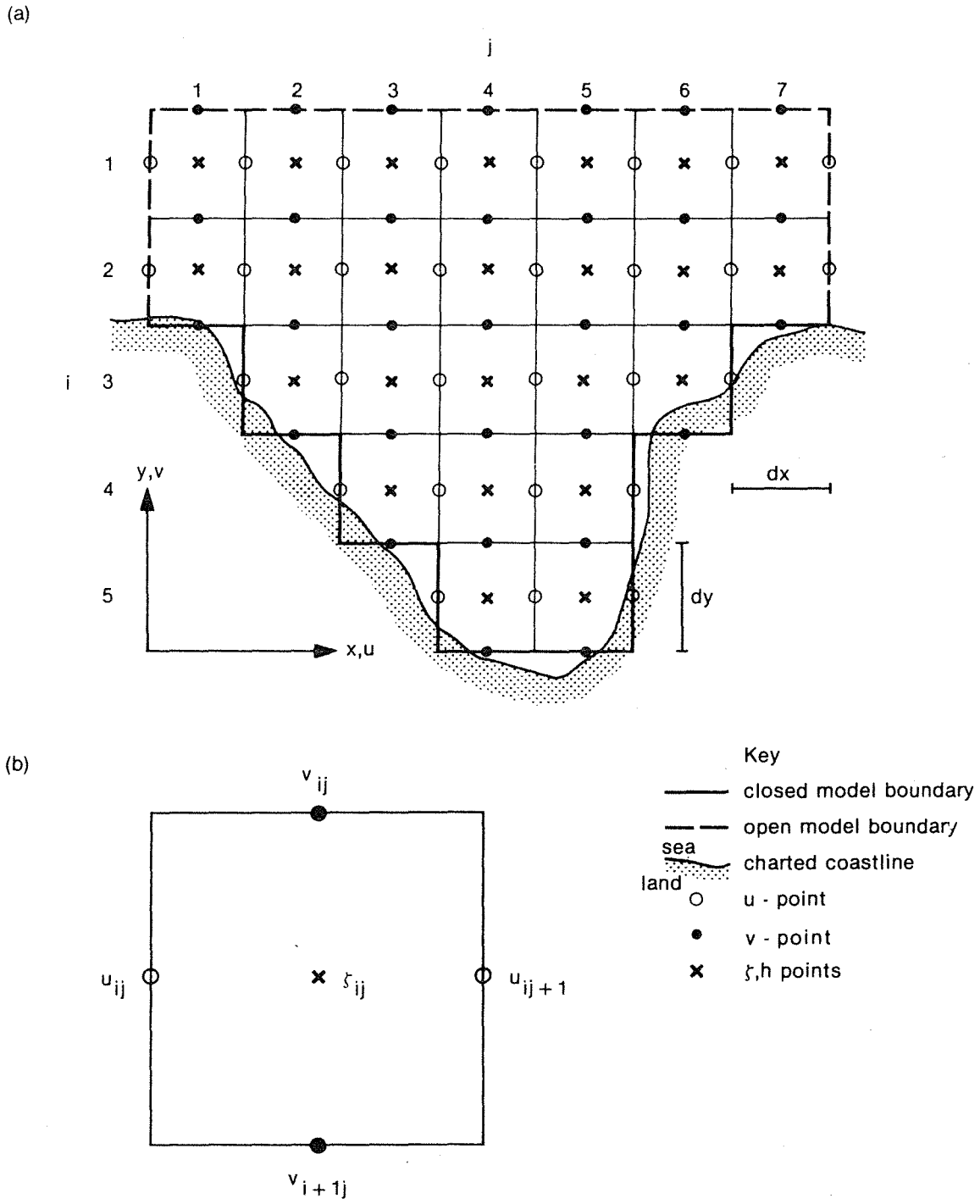

Figure 1 : Schematic display of (a) the model grid system for a water body with open and closed boundaries, (b) a single cell of the model grid system showing locations of defined variables.

Following Flather and Heaps (1975), the basic equations (1)-(3) may be approximated in explicit finite-difference form. A simplified scheme is first given, in which the momentum advection terms are neglected. The finite-difference approximations are then:

$$[\zeta_{ij}(t+\Delta t) - \zeta_{ij}(t)]/\Delta t = -[d_{ij+1}(t)u_{ij+1}(t) - d_{ij}(t)u_{ij}(t)]/\Delta x$$

$$- [e_{ij}(t)v_{ij}(t) - e_{ij+1}(t)v_{ij+1}(t)]/\Delta y \ , \qquad (4)$$

$$[u^*_{ij}(t+\Delta t) - u_{ij}(t)]/\Delta t = f\tilde{v}_{ij}(t) - g[\zeta_{ij}(t+\Delta t) - \zeta_{ij-1}(t+\Delta t)]/\Delta x$$

$$- ku^*_{ij}(t+\Delta t)[u^2_{ij}(t) + \tilde{v}^2_{ij}(t)]^{1/2}/d_{ij}(t) + \tau^x_{ij}/\rho d_{ij}(t) \ , \qquad (5)$$

$$[v^*_{ij}(t+\Delta t) - v_{ij}(t)]/\Delta t = -f\tilde{u}_{ij}(t+\Delta t) - g[\zeta_{i-1j}(t+\Delta t) - \zeta_{ij}(t+\Delta t)]/\Delta y$$

$$- kv^*_{ij}(t+\Delta t)[\tilde{u}^2_{ij}(t) + v^2_{ij}(t)]^{1/2}/e_{ij}(t) + \tau^y_{ij}/\rho e_{ij}(t) \ , \qquad (6)$$

where Δx, Δy is the grid spacing

Δt is the computational time step

u^*_{ij}, v^*_{ij} are the velocity components updated by all but the momentum advection terms, and

$$d_{ij} = \tfrac{1}{2}(H_{ij} + H_{ij-1}), \quad e_{ij} = \tfrac{1}{2}(H_{i-1j} + H_{ij}),$$

$$\tilde{u}_{ij} = \tfrac{1}{4}(u_{ij} + u_{i-1j} + u_{i-1j+1} + u_{ij+1}),$$

$$\tilde{v}_{ij} = \tfrac{1}{4}(v_{ij} + v_{i+1j} + v_{i+1j-1} + v_{ij-1}).$$

When the changed values of velocity components due to other dynamic processes have been calculated from equations (5) and (6), the advection of momentum terms may then be estimated and included by addition. The 'angled-derivative' method of Roberts and Weiss (1966) is used to approximate spatial derivatives of the velocity components as finite-differences properly centred in space and time. Thus for the x-directed component of velocity, momentum advection effects are included as follows:

$$[u_{ij}(t+\Delta t) - u^*_{ij}(t+\Delta t)]/\Delta t =$$

$$- \frac{1}{2\Delta x} u^*_{ij}(t + \Delta t).\{u^*_{ij+1}(t + \Delta t) - u^*_{ij}(t + \Delta t) + u_{ij}(t + \Delta t) - u_{ij-1}(t + \Delta t)\}$$

$$- \frac{1}{4\Delta y} [\{v^*_{ij}(t + \Delta t) + v^*_{ij-1}(t + \Delta t)\}.\{u_{i-1j}(t + \Delta t) - u_{ij}(t + \Delta t)\}$$

$$+ \{v^*_{i+1j}(t + \Delta t) + v^*_{i+1j-1}(t + \Delta t)\}.\{u^*_{ij}(t + \Delta t) - u^*_{i+1j}(t + \Delta t)\}] \qquad (7)$$

This equation is written for the case where calculations at successive points in the u subgrid are proceeding row-wise from top left to bottom right. It is recommended by Roberts and Weiss (1966) that the order of calculation through the grid points be reversed at each successive time step. This calls for a modification to equation (7): in difference expressions the symbols u and u* should then be interchanged. Similar equations can be written for the y-component of velocity, with momentum advection included. These formulae cannot be applied to points closer than one cell width from the open sea boundaries since some of the input quantities required are then undefined; at these points the momentum advections effects must be neglected.

In conjunction with specified conditions at the model boundaries, the numerical scheme is used to advance the solution over successive time steps of length Δt, commencing from known initial conditions $\zeta_{ij}(0)$, $u_{ij}(0)$, $v_{ij}(0)$.

3.1 Boundary Conditions

The boundaries of the model are delineated by grid cell walls. They fall into two categories: closed boundaries, representing coastlines, and open boundaries, representing the non-coastal limits of the modelled ocean area.

At closed boundaries the normal component of depth-averaged velocity is set to zero, a condition of no flow across the model coastlines.

A number of alternative open boundary specifications may be made, depending on the data available, and the specific modelling application:

- water elevation data may be supplied at grid cells located adjacent to open boundaries,
- water level gradients normal to the open boundaries may be defined,
- volume flux (or vertically-averaged velocity) components normal to open boundaries may be specified, or
- 'radiation conditions' may be formulated, which allow internally generated disturbances to propagate outwards normally across open model boundaries in the form of long shallow-water waves.

The choice of open boundary conditions is critical. Selection of appropriate types of boundary conditions ensures not only that the model solution is stable, but also that the desired range of physical processes are represented in the solution. The accuracy with which the open boundary conditions are specified affects the accuracy of the solution (often much more than approximations made in the finite-difference scheme). Inaccuracies may be

minimised in the region of principal interest by locating the open boundaries sufficiently far away.

4. MODEL IMPLEMENTATION

Initial decisions to be made in implementing the model relate to the area covered by the model, the orientation and spatial resolution of the model grid and the length of the computational time step to be used. The choice of spatial resolution is influenced by the form and size of the water body, and the type of issue being addressed by the modelling exercise. A constricted water body with irregular coastline and channels would require modelling with a finer resolution than for an open water body of smoothly varying bathymetry. Assessment of changes in coastal water flow patterns due to the installation of a proposed maritime structure may require a model of high resolution.

The computational time step Δt must be small enough to ensure that the model solution remains stable. The stability criterion of Courant, Friedrichs and Lewy (1928), applicable for explicit finite-difference schemes, states that

$$\Delta t < \min(\Delta x, \Delta y)/(2gh_{max})^{1/2}, \qquad (8)$$

where h_{max} is the maximum water depth defined in the model.

For a given area modelled and a given time period of simulation, a doubling in spatial resolution leads to a four-fold increase in the number of grid cells employed and, by virtue of the stability criterion, an eight-fold increase in computing effort. Thus, the investigator is frequently forced to reach a compromise between grid resolution and computer costs incurred in running the model.

Once these decisions have been made the preparation of input data files describing the planform and bathymetry of the modelled area may proceed. A best fit schematisation of the charted coastline can be derived using x- and y-directed line segments of a scaled grid superimposed on hydrographic charts of the study area. A code number can then be assigned to each grid cell to show whether the cell represents an area of land or water, and to indicate the disposition of closed and open boundaries. Collectively these numbers form a matrix which represents the planform of the modelled area. An input matrix of bathymetry can also be constructed by assigning an effective average water depth to each of the grid cells. For the purposes of the model these depths should be referred to a mean sea level datum.

Basically the model calculates the changes in water level and velocity which occur over successive time intervals. It is therefore necessary to supply starting values, known as the initial conditions of the solution, at the commencement of each model simulation. The initial conditions may reflect a knowledge of the motion at a given instant; for example, they may be derived either from the final results of an earlier model run, or from detailed field measurements. In this case the initial solution would be consistent with the history of the forcing and the boundary conditions applied. If no prior knowledge about the motion exists, the model solution must be allowed to develop from some arbitrary initial condition, for example, a state of undisturbed equilibrium. The mismatch which then exists between the initial conditions, the boundary conditions and the applied forcing causes impulsive excitation of the natural wave modes of the model region. These waves tend to be internally reflected at the open model boundaries (unless the radiation

condition is employed) and it may take some considerable time for them to decay away through the action of bottom friction.

One way of reducing the computational effort required to obtain a satisfactorily adjusted solution is to minimise the size of the initial transient disturbance. This may be achieved by applying to the boundary and forcing conditions a linear ramp function of time of the form:

$$r = \begin{cases} t/T & 0 < t \leq T \\ 1 & t > T \end{cases}, \qquad (9)$$

where T is the time duration of the ramp. Such an approach has been used with success by Hunter (1982), Bode et al. (1981), and again in this model development.

The form of the bottom stress term in the vertically-integrated equations appears to be inadequate for very shallow water in that, as the total water depth tends to zero, the bottom stress term becomes very large. This problem is overcome in the model by redefining the denominator of this term as the maximum of the water column depth and a predetermined depth.

The results of the model may be output as fields (spatial distributions) of the water levels or velocities at selected times, or as detailed histories of these variables at selected locations. The velocities may be converted to volume flux rates, if required. Water velocities, transports and elevations may be time-averaged to examine the residual water drifts and the distribution of mean sea level. The bottom stress distribution may be estimated, as may the rate at which the current performs work against the bottom stress. The latter quantity is related to the energy available for vertical mixing of the water column.

5. MODEL TESTING

The numerical model developed in this study has to be capable of incorporating a range of hydrodynamic processes, operating within a water body of irregular form, and driven by several simultaneous forcing effects. In order to gain confidence in the results produced by the model, a series of verifiable tests were devised.

The model was used to simulate long, shallow water waves in rectangular channels and bays of constant depth. The motions chosen were:

- plane, frictionally-damped progressive waves in a rectangular channel,
- damped, progressive Kelvin waves (see Lamb 1932, Art. 208) in a rectangular channel,
- plane, damped 'standing' co-oscillations in a rectangular bay,

for each of which an analytic solution is known. These waves, of maximum amplitude 0.5 m and of period 12 hours, were simulated on a rectangular area, 30 km x 60 km, with a computational grid spacing of 5 km, a uniform water depth of 30 m, and a time step of 3 minutes. A linear bottom friction term was used in the model. Several formulations of the open boundary conditions were tested. Excellent agreement between modelled and theoretical results was obtained, generally within 1%.

In another set of tests the orientation of the rectangular bay was changed with respect to a fixed computational grid. Successive runs of the model with the mouth of the bay opening in the x-positive, x-negative; and y-negative directions yielded the identical motion.

The model was tested for a simple case of wind forcing. A water body, bounded by one straight coast and three open sea boundaries, was considered, with isobaths straight and parallel to the coastline. A steady, uniform wind stress in the long-shelf direction was applied to the initially static water mass. The open boundary conditions set were zero elevation along the outer sea boundary, and zero normal elevation gradients at the cross-shelf open boundaries. The results showed that the long-shelf depth-averaged current speed tended everywhere toward a constant, limiting value at which the bottom stress was in balance with the wind stress. However, the time scale for establishment of this speed was shown to be directly proportional to the local water depth; that is, the zone of steady-state flow extended offshore with time. A cross-shelf water surface slope developed in dynamic balance with the Coriolis force acting perpendicularly to the long shelf flow. These results are consistent with the analytic solution of the frictional adjustment problem for this case (Csanady 1982), although Csanady did not invoke a boundary condition at a finite distance from the coast as was done in the numerical model. Nonetheless, quantitative agreement was obtained for both the steady state current velocity and for the establishment times at various depths.

6. DAMPIER ARCHIPELAGO TIDAL SIMULATION

6.1 General

The first application of the model aimed to simulate the mean spring tides and tidal currents of the nearshore and adjacent North-West Shelf waters off Dampier, Western Australia (see Figures 2 and 3). The Dampier Archipelago (Figure 4) offers one of the more sheltered areas of navigable, near-shore water along this coast, and has allowed the development of port facilities over the past 20 years to handle the export of salt and iron ore. Further port development has commenced recently, following the discovery offshore of hydrocarbons. The environments of the Dampier Archipelago are of considerable value for recreation and conservation.

The oceanic tide off the north-west coast of Australia has dominant constituents at periods of 12.0(S2) and 12.4(M2) hours (Easton 1970). Particularly large tides occur when the M2 and S2 constituents reinforce. These are referred to as spring tides. They occur at approximately fortnightly intervals near times when the sun, moon and earth are aligned. Tidal motions on continental shelves and in coastal waters are basically co-oscillations forced by the deep oceanic tide: the response of these water bodies to direct astronomic forcing is insignificant (e.g. Garrett 1975).

The North-West Shelf (Figure 2) is straight and extends for more than 1000 km from North-West Cape, where it is about 10 km wide, to north of Broome, where it is about 170 km wide. The semi-diurnal tidal amplitude increases long-shelf in the direction of increasing shelf width, and Holloway (1983) has demonstrated that the associated pressure gradient force can account for the observed long-shelf component of the semi-diurnal tidal currents.

Holloway (1982, 1983) has reported that North-West Shelf waters off Dampier are vertically well-mixed in winter, while in summer a marked thermocline develops. He has shown that, even in the presence of the summer

stratification, tidal currents on the inner and mid shelf are predominantly barotropic, i.e. there is little vertical shear. Inshore waters (depths of 20 m or less) are generally well-mixed (D.C.E, unpublished data). Horizontal density gradients are dynamically insignificant for the tidal motions considered here.

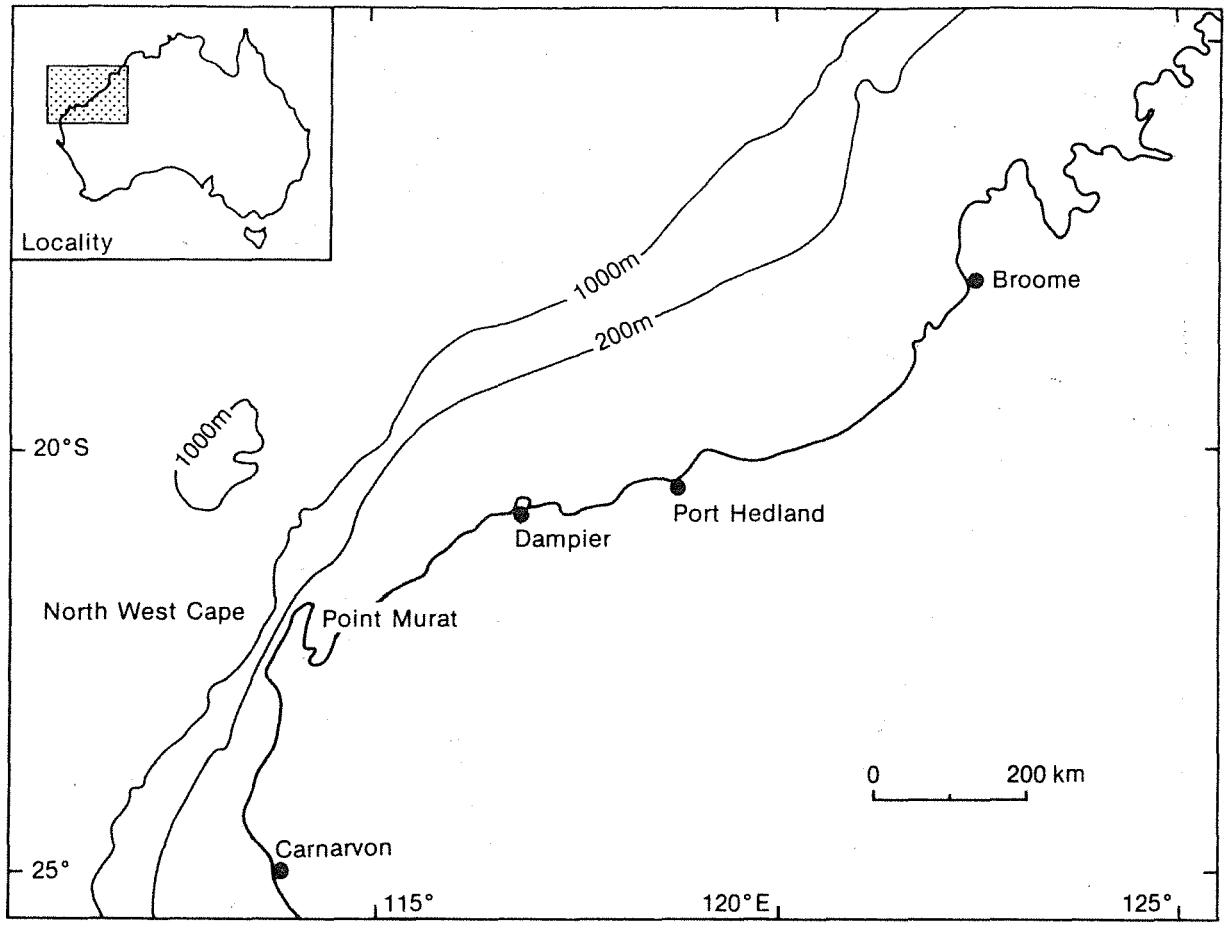

Figure 2 : The North-West Continental Shelf of Australia.

6.2 Area Modelled

As shown in Figure 3, the area modelled is situated within a rectangle extending some 87 km across the North-West Shelf out to the vicinity of the 60 m depth contour, and 102 km in a long-shelf direction (065^0 N) from Cape Preston to east of Legendre Island. The modelled area is enclosed by one land boundary and three water (open) boundaries, which will be referred to as the SW, the NE and the outer (long-shelf) open boundaries.

This area was chosen to cover the transition from smoothly varying flow on the open shelf to the current patterns of coastal waters within the Archipelago, which are strongly conditioned by the orientation of coastlines, submarine shoals and deeper channels. The open boundaries of the model were set far from the Dampier Archipelago to minimise any errors in the model results arising from inaccuracies in the specification of boundary conditions. The outer, long-shelf boundary was located to make use of known tidal constants derived (Holloway 1983) from sea bed tide gauge 1 (Figure 3) moored at a depth of 61 m.

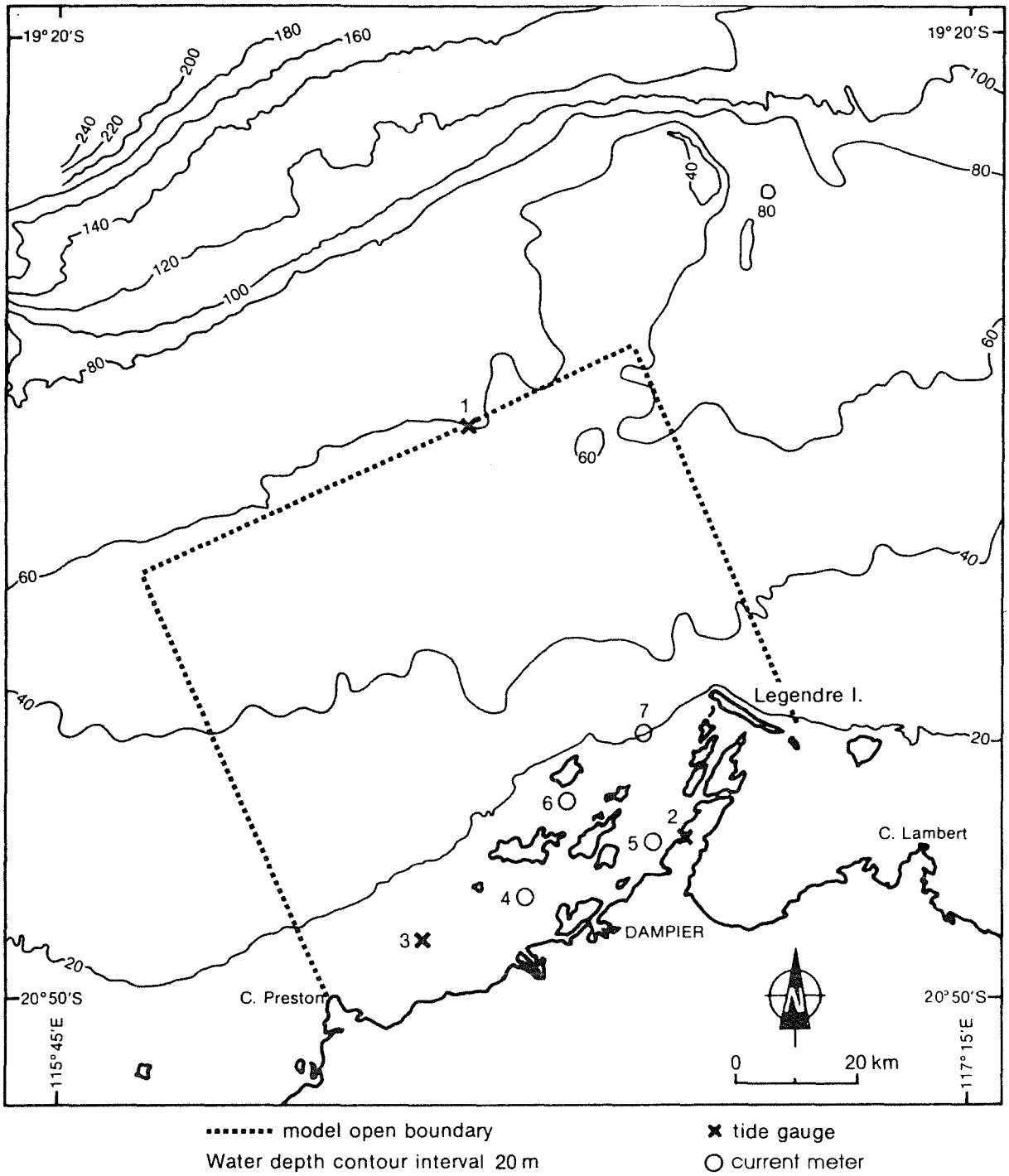

Figure 3 : The Dampier Archipelago and adjacent North-West Shelf waters. Bathymetry, the locations of moored instruments and the extent of the modelled area are shown.

6.3 Model Layout

A model grid spacing of 3 km was chosen, this being just small enough to enable resolution of the major geographic and bathymetric features of the Archipelago. RAN hydrographic charts (AUS742 1982, AUS741 1983, AUS58 1983) of the area were used to prepare the model layout, which consists of 909 active grid cells, each representing a 9 km^2 area of water. The largest water depth represented in the model is 69.7 m. Figure 5 shows the arrangement of closed and open boundaries, and selected bathymetric contours (referenced to mean sea level, Dampier) derived from the estimated mean depths for each grid cell.

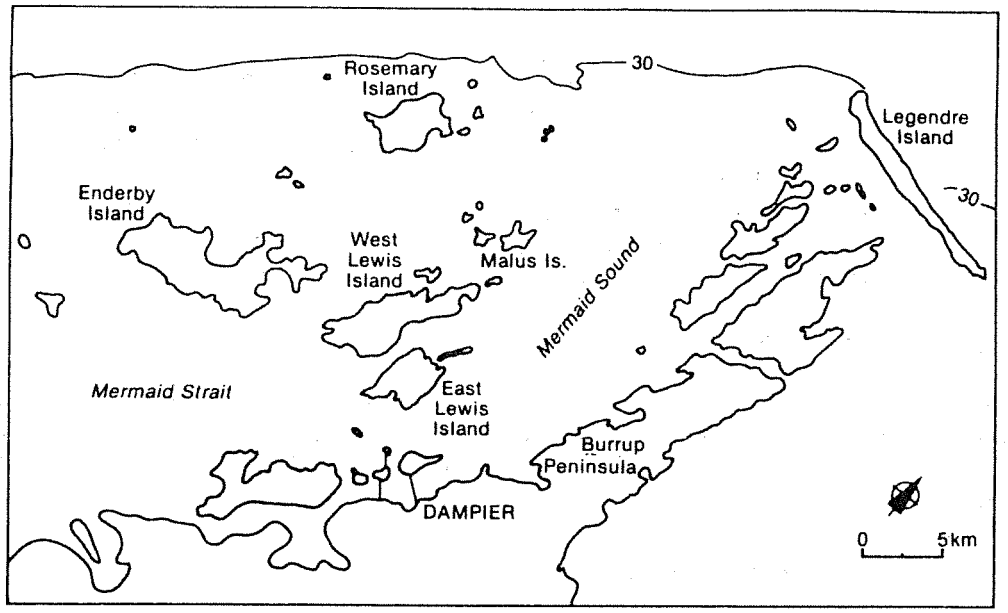

Figure 4: The Dampier Archipelago. Place names and the 30 m depth contour are shown.

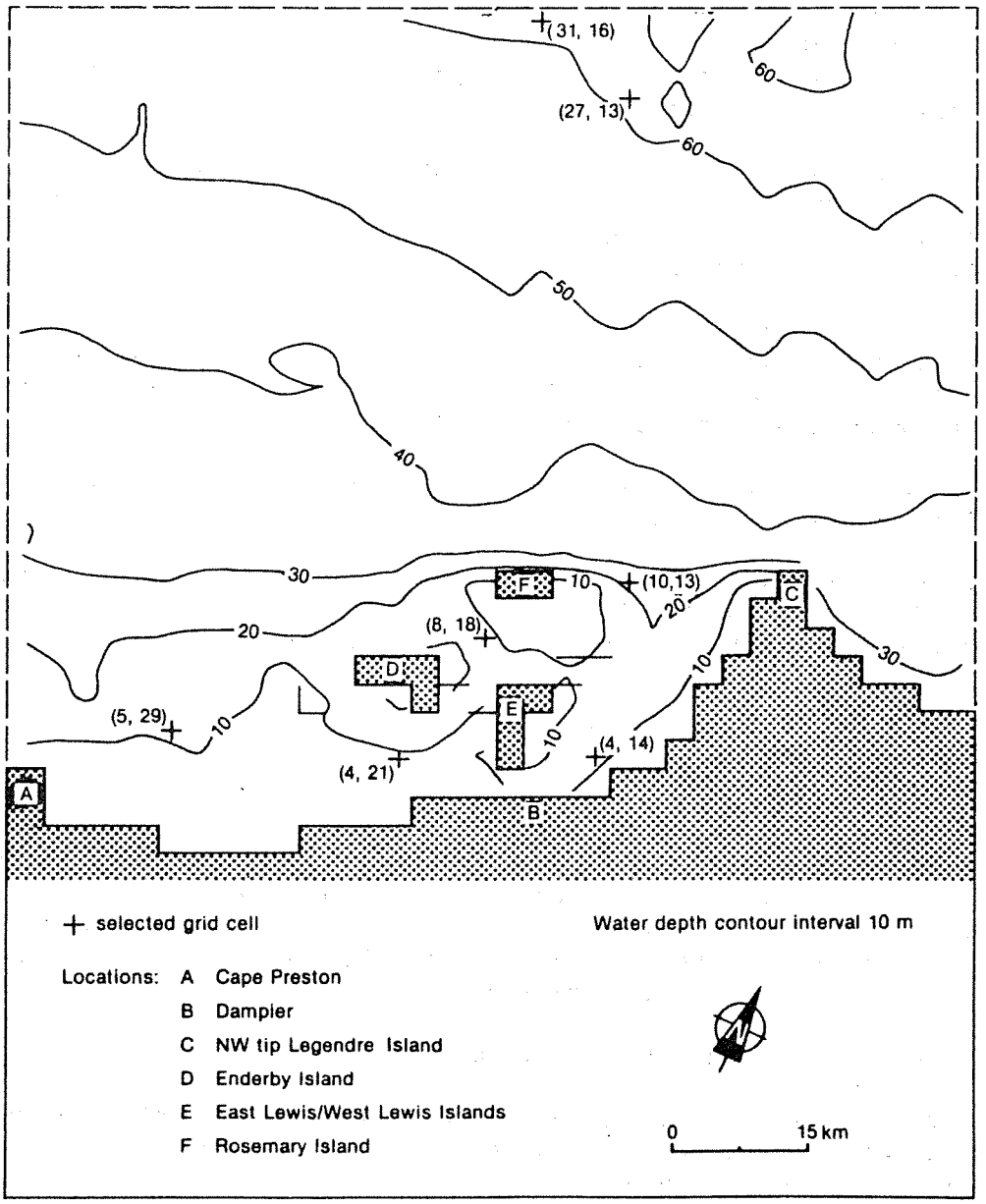

Figure 5: Schematised coastline, open boundaries and bathymetry used in the model. Selected grid cells referred to in the text are shown.

One disadvantage of this layout is that some of the main interisland channels are represented widthwise by only one grid cell. Therefore it was not possible to evaluate accurately the momentum advection terms near these channels. Other smaller but locally important channels were not included at all. The implementation of a model of finer resolution would resolve these difficulties. However, as a first approach, the relatively coarse 3 km grid was used to contain the amount of computation involved.

6.4 Open Boundary Conditions

The tidal co-oscillations and currents of this region were modelled using open boundary conditions appropriate to mean spring (M2 + S2) tides. Water levels were prescribed adjacent to the outer, long-shelf boundary as a function of the form,

$$\zeta = A.\exp(-1x).\cos(\frac{2\pi t}{T}) \quad , \tag{10}$$

where

- the value of the local tidal amplitude (A) was derived from an harmonic analysis (Holloway 1983) of 90 days' data from sea bed tide gauge 1, located on the outer open boundary (Figure 3)

- the exponential term was used to represent the long-shelf (x) variation of the tidal amplitude. Holloway (1983) estimated the value of the constant 1 in the exponent as (2 to 2.5) x 10^{-6} m^{-1} for both M2 and S2 tides, for observations between Carnarvon and Broome

- the water level phase was assumed constant along the outer open boundary. Known semi-diurnal tidal constants from alongshore stations, and the results of Schwiderski's (1979) world ocean numerical tidal model (see Holloway 1983) support this assumption

- the water level was allowed to vary sinusoidally with a period T, between the actual M2 and S2 periods.

At each of the cross-shelf open boundaries, use was again made of the long-shelf variation of tidal amplitude. The boundary conditions were specified as the finite-difference form of the relationship

$$\frac{\partial \zeta}{\partial x} = - 1\zeta \quad , \tag{11}$$

and thus no information concerning variations in the cross-shelf direction was introduced. These seem reasonable conditions for the mid-continental shelf. Their validity for near coastal waters is less certain, but it should be remembered that the cross-shelf open boundaries were located away from the areas of principal interest to minimise the influence of any inaccuracy in the boundary specification on the solution.

6.5 Model Procedure and Initial Conditions

Because of the problems in evaluating the non-linear momentum advection terms in the vicinity of narrow interisland channels, the model was run with these terms set everywhere to zero.

The Courant-Friedrichs-Lewy stability criterion (see equation (8)) required that the computational time step should not exceed 81 seconds for this application. The time increment used was 62.8 seconds. A complete tidal period was defined to consist of exactly 700 time steps.

Water elevations and velocities were set to zero everywhere at the commencement of the model calculations, to represent an initial state of static equilibrium. The model was run for a total of twelve tidal cycles. For an initial period of one and a half cycles the seaward boundary data were multiplied by a linear ramp function of time ((see equation (9)) to reduce initial transient disturbances. The computing was performed on the Western Australian Regional Computing Centre's DEC System-10 machine and took 44 minutes central computing time.

A complete list of the model parameter values used is as follows:

Grid size ($\Delta x = \Delta y$)	3000 m
Time step	62.8 s
Tidal period	43939.2 s
Coriolis parameter	-0.5×10^{-4} s^{-1}
Bottom friction coefficient	0.0025
Gravitational acceleration	9.81 ms^{-2}
Long-shelf tidal decay constant	2.0×10^{-6} m^{-1}
Reference mean spring tidal amplitude	1.54 m

6.6 Model Results

6.6.1 Convergence of the Model Solution

The solution for the interior motion should converge to a cyclic behaviour in response to a cyclic water level forcing at the model open boundaries. Results obtained from two selected grid cells were used to evaluate the rates of convergence. Grid cell (4,14) represents a location well within Mermaid Sound at a depth of 8 m. Grid cell (27,13), with a depth of 52.5 m, lies near the outer seaward boundary of the model. Water elevation and velocity component values were each compared at the same stage of successive tidal cycles. For water depths of about 10 m, convergence had essentially occurred by the end of the sixth cycle. In the deeper, outer extremities of the model, about twelve tidal cycles were required to obtain convergence of velocities to about 2%, even though the elevations had converged much sooner. These convergence times are longer than is often reported in the literature (e.g. Pingree & Maddock 1977, Fandry 1981). It is thought that this is because of the use here of the normal gradient of elevation condition at the cross-shelf open boundaries; direct specification of water elevations is more commonly applied.

For steady cyclic motion there should be no nett loss or accumulation of water over a tidal cycle. The tidally-integrated volume transports across the open boundaries were calculated for the twelfth cycle. As indicated in Table 1, the calculated rate of nett volume change was three orders of magnitude lower than the tidally-integrated volume transport rates across the individual open boundaries, demonstrating that a desirable balance had been achieved.

TABLE 1

Modelled Volume Flux Balance for the Twelfth Tidal Cycle

Tidally-averaged Rate of Volume Outflux (m^3s^{-1})			
SE Boundary	NE Boundary	Outer Boundary	Nett
-33.06	70.53	-37.49	-0.02

6.6.2 The Spatial Structure of the Model Solution

Figures 6(a)-(d) show the spatial structure of the solution for the surface tide at four times during the twelfth tidal cycle. These times correspond to the occurrence at the outer long-shelf open boundary of mean sea level (falling), low water, mean sea level (rising) and high water. The long-shelf variation in the tidal amplitude is clearly seen in Figures 6(b) and 6(d) and complies with the conditions imposed at the open boundaries. The model predicted cross-shelf amplification of the surface tide. For example, Figure 6(d) shows a cross-shelf increase in tide height from 1.54 m on the shelf at the outer boundary of the model to 1.81 m near the town of Dampier.

Tidal elevations in shallow coastal waters lag slightly behind the elevations on the shelf. Figure 6(a) shows that on a falling tide, when mean (zero) sea level is attained at the outer boundary, the water levels within the Archipelago are still positive. Surface elevation gradients are largest around the outer reaches of the Archipelago, with the exception of the entrance to Mermaid Sound, where these gradients diminish to the north-east. Figure 6(c) shows the lag of coastal water levels behind those on the shelf for a rising tide. In the longshore direction there is very little apparent phase variation in the surface elevation.

The modelled tidal current results are presented for a sub-area of the model, centred on the Dampier Archipelago. Current velocities elsewhere vary smoothly since they are in open water and not subject to irregular coastlines.

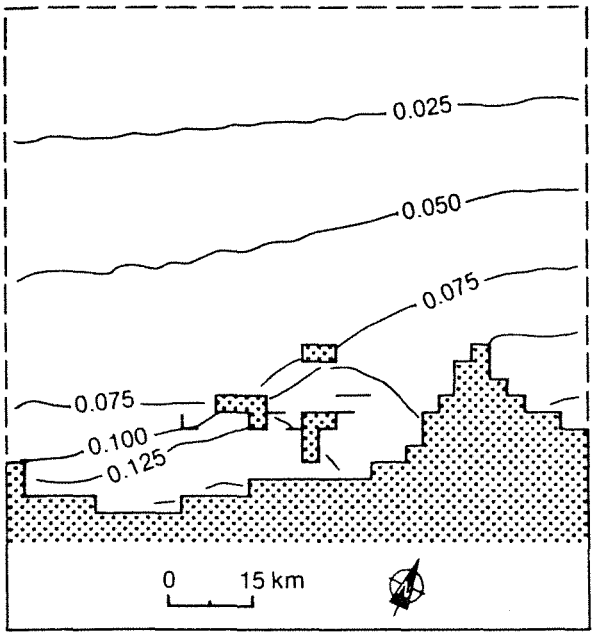

(a) Water level contour interval 0.025 m
11.25 tidal cycles elapsed.

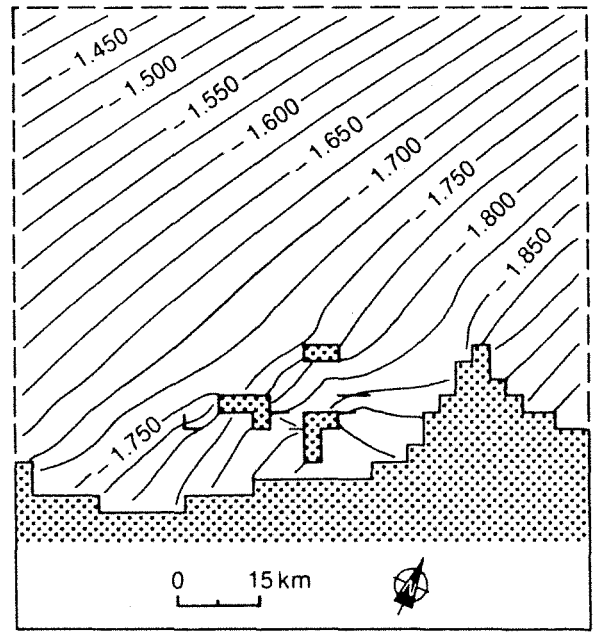

(b) Water level contour interval 0.025 m
11.5 tidal cycles elapsed.

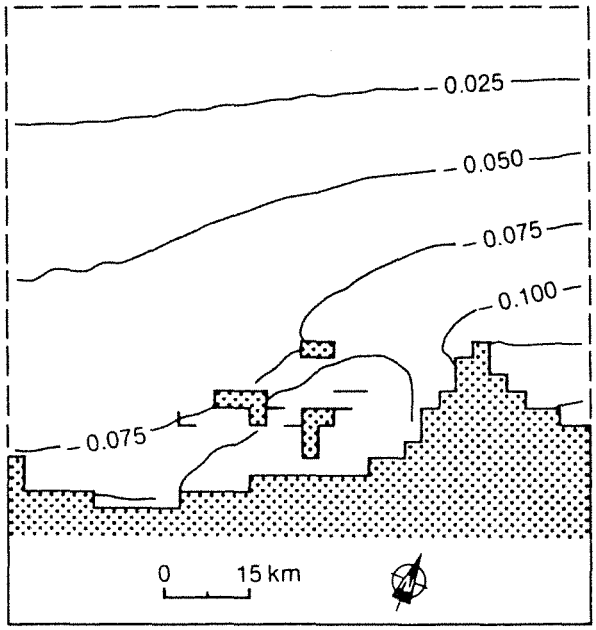

(c) Water level contour interval 0.025 m
11.75 tidal cycles elapsed.

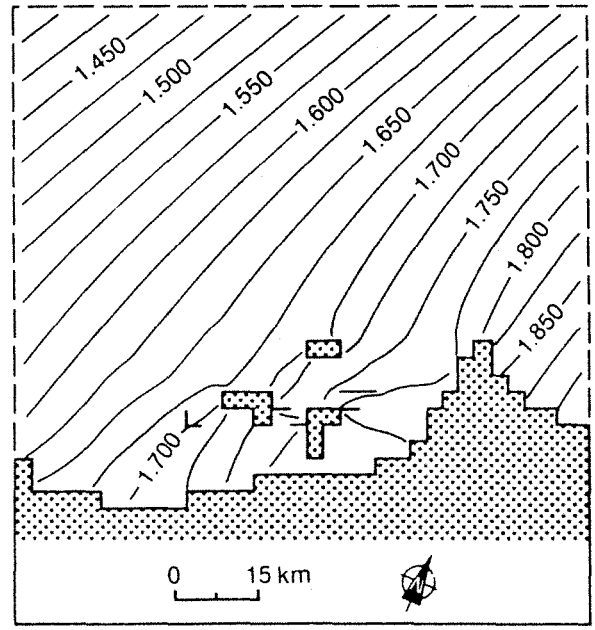

(d) Water level contour interval 0.025 m
12 tidal cycles elapsed.

Figure 6 : The spatial field of water level computed at (a) 11.25, (b) 11.5, (c) 11.75, (d) 12 elapsed tidal cycles from model run commencement.

Figure 7(a) represents an ebb tide situation. The water retreats obliquely across the continental shelf, setting on average at about 300^0 N, and being directed slightly more cross-shelf toward the outer extremity of the model where speeds of about 35 cm s^{-1} are achieved. Water moves seaward across all of the entrances to the Archipelago. Considerable curvature occurs at the entrance of Mermaid Sound, which is oriented almost perpendicularly to the principal ebb direction on the shelf. The strongest ebb movements of Archipelago waters occur near its seaward entrances. Ebb currents reach 75 cm s^{-1} off the SW end of Enderby Island; 60 cm s^{-1} between Rosemary and Enderby Islands, and 45 cm s^{-1} in relatively shallow water at the western side of the entrance to Mermaid Sound. Velocities diminish in a NE direction

across the entrance of the Sound before increasing again outside the northern tip of Legendre Island. The area of lowest speed at this time occurs at the head of Mermaid Sound near the town of Dampier.

Figure 7(b) shows that, at reference low water, the tidal currents on the shelf are weak, and rotating rapidly anticlockwise. A coherent pattern of outflowing currents with speeds of up to 15 cm s^{-1} still persists in Mermaid Sound, whereas in the southern portion of Mermaid Strait, inflowing currents have just commenced. Flow through the channel south of East Lewis Island is at this time near maximum at 20 cm s^{-1} in an ENE direction.

The directions of flood currents, shown in Figure 7(c), are opposite to the ebb directions and their speeds stronger (increasingly towards the seaward open boundary), but the main features of the patterns are otherwise similar.

Figure 7(d) shows that at the time of reference high water, movement on the shelf is weak and in transition. A pattern of weak incoming current persists throughout Mermaid Sound even though water in southern Mermaid Strait is beginning to ebb. In the channel south of East Lewis Island the current is near maximum (16 cm s^{-1}) in a WSW direction.

6.6.3 The Time Dependence of the Model Solution

Computed time histories of tidal elevations, current speeds and directions at selected grid cells of the model are displayed in Figure 8.

Figure 8(a) provides a comparison of the time series variations for three locations aligned in a cross-shelf direction. These locations (shown in Figure 5) are, inner Mermaid Sound (grid cell (4,14)), Mermaid Sound entrance (grid cell (10,13)), and on the continental shelf near the outer model boundary (grid cell (27,13)). The cross-shelf amplification of the vertical tide is shown. Inshore water elevations lag shelf water elevations by about ten minutes. Peak tidal speeds show a general increase in the off-shore direction, with peak flood speeds becoming progressively more dominant over peak ebb speeds. Significant ebb and flood tidal currents persist in Mermaid Sound at times when currents on the shelf are weakening and rotating. Peak ebb current in the inner reaches of Mermaid Sound is delayed by 100 minutes with respect to peak ebb current near the outer boundary of the model. However, peak flood current in Mermaid Sound precedes peak flood current on the shelf by about 35 minutes. The inshore transition from peak ebb to peak flood current thus occurs in little more than one quarter of the tidal period. The current speed minima occur in Mermaid Sound up to 35 minutes later than on the continental shelf.

Figure 8(b) shows time histories from three locations long-shore; inner Mermaid Sound (grid cell (4,14)), Mermaid Strait (grid cell (4,21)) and a location 40 km south-west of Dampier (grid cell (5,29)). Tidal elevation amplitudes decrease slightly to the SW, and there appears to be very little long-shore phase variation. Peak currents increase to the south-west and the times of occurrence of peak speeds differ markedly. Peak ebb current in Mermaid Strait occurs about 130 minutes before that in Mermaid Sound and about 15 minutes before that further to the SW. Peak flood current in Mermaid Strait precedes that in Mermaid Sound by about 20 minutes, and that further to the SW by about 15 minutes. In Mermaid Strait the transition from peak ebb to peak flood is slightly more rapid than from peak flood to peak ebb, but this effect is less pronounced than for inner Mermaid Sound.

Figures 8(a) and 8(b) suggest the presence in the model solution of frequencies higher than the fundamental semi-diurnal frequency. These higher

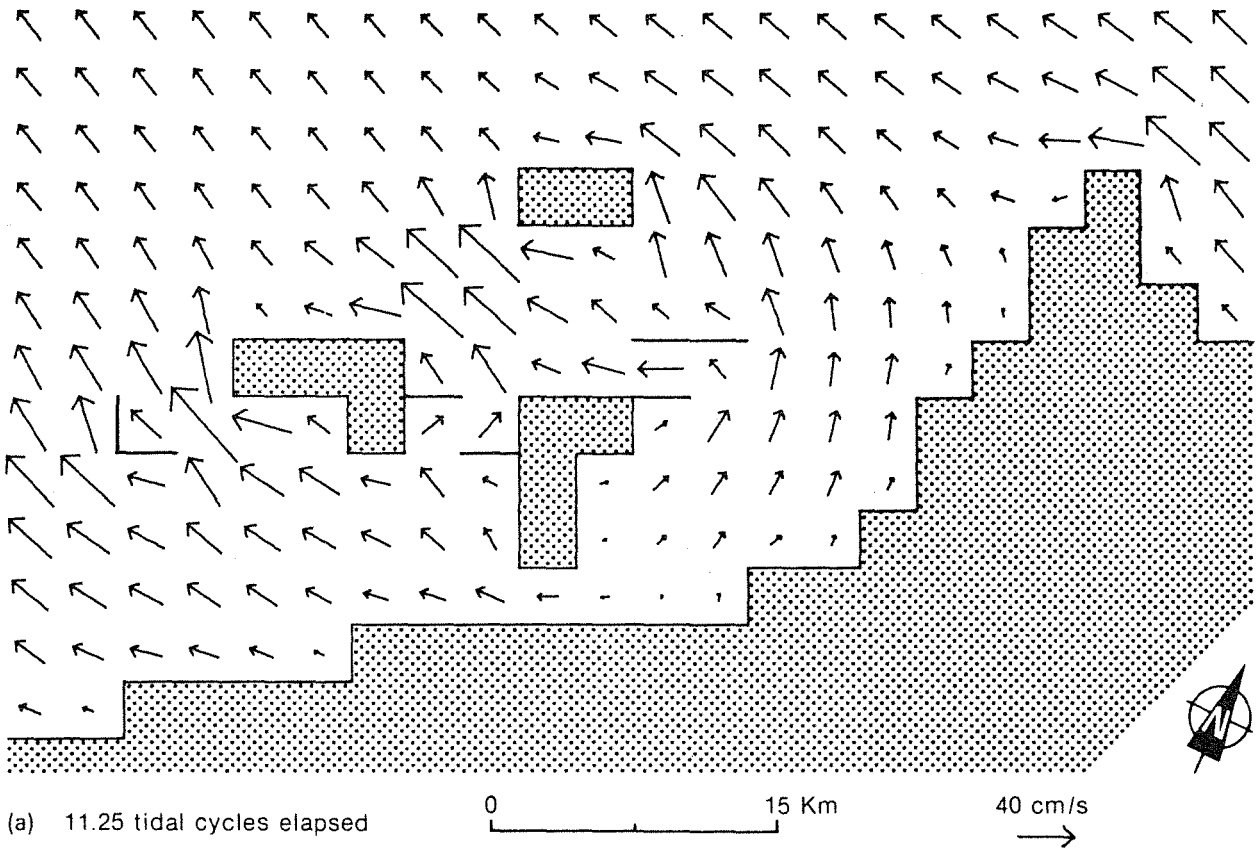

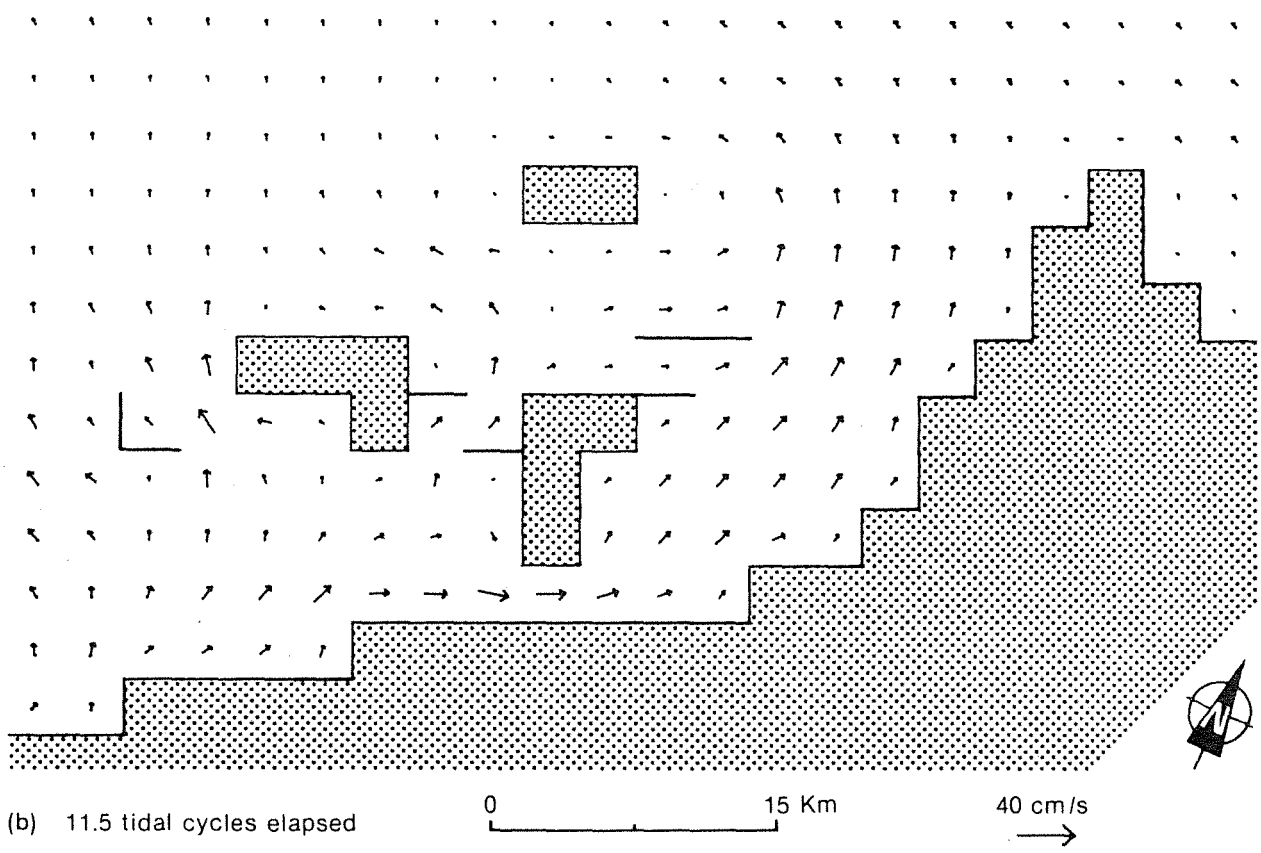

Figure 7 : The spatial field of depth-averaged tidal currents computed at (a) 11.25, (b) 11.5, (c) 11.75, (d) 12 elapsed tidal cycles from model run commencement.

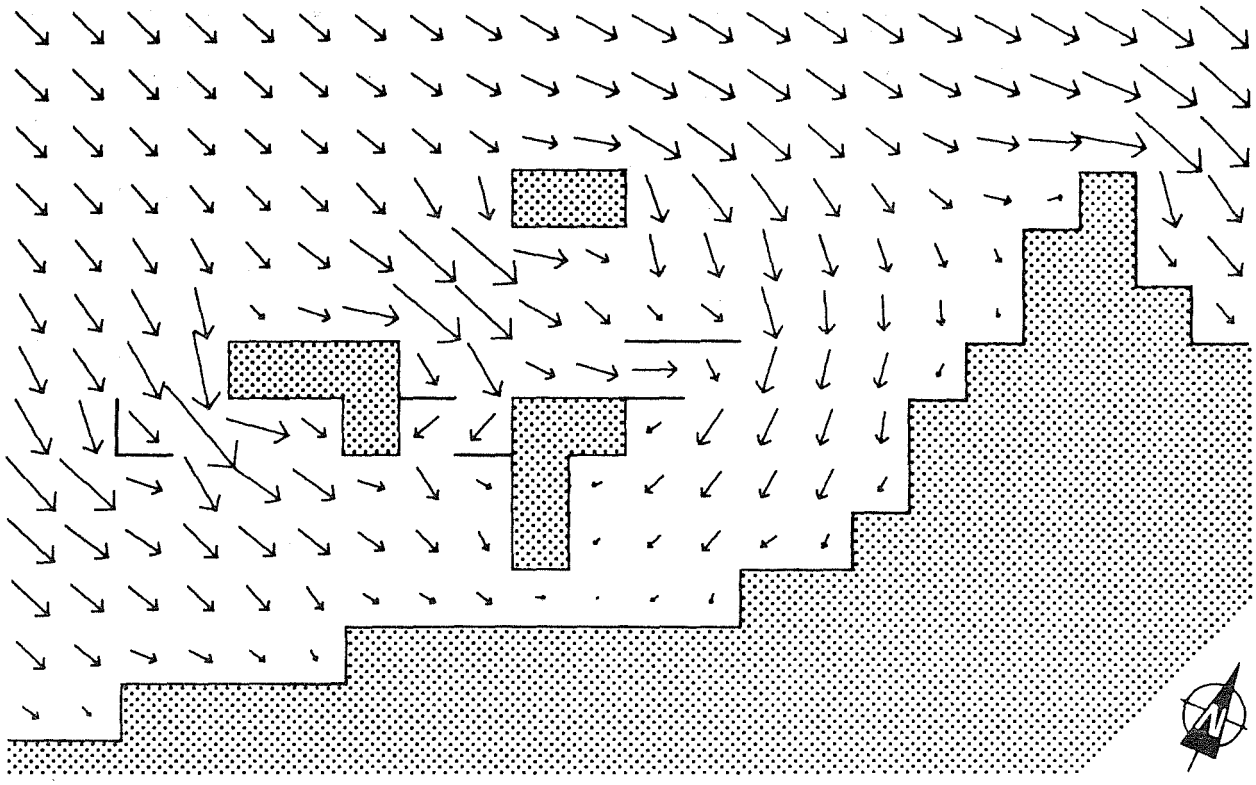

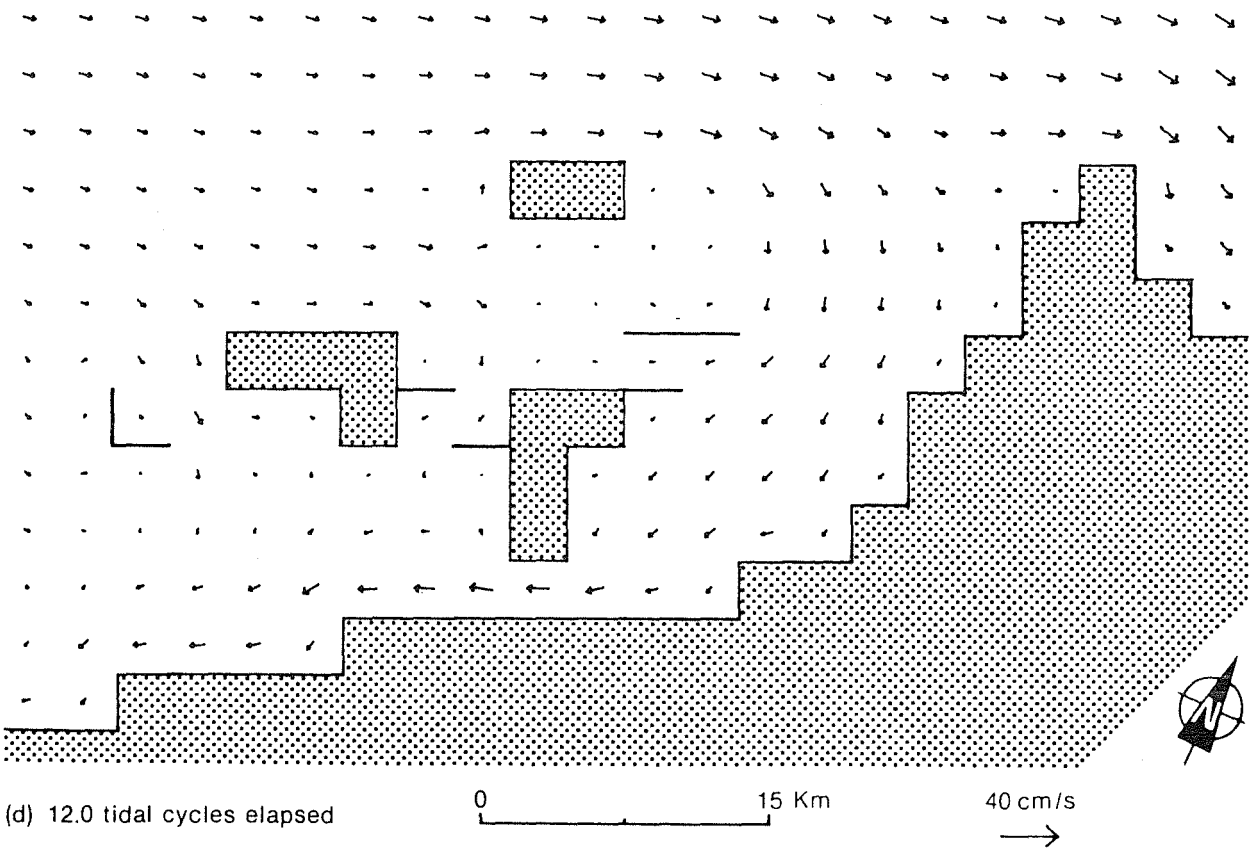

Figure 7 : The spatial field of depth-averaged tidal currents computed at (a) 11.25, (b) 11.5, (c) 11.75, (d) 12 elapsed tidal cycles from model run commencement.

frequencies are particularly evident in the time histories of tidal currents in shallow waters, e.g. at grid cell (4,14), and are to a large extent responsible for the timing of the peak current speeds and the more rapid reversal from ebb to flood flows in shallow water locations. They arise through the action of non-linear processes. The non-linearity in the continuity equation can give rise to even harmonics, while the quadratic bottom stress term can generate both even and odd harmonics (Gallagher and Munk 1971).

A Fast Fourier Transform algorithm was applied to each of the solution time-series obtained. This transform technique analysed the discrete solution as a sum of sinusoidal terms with frequencies equal to a fundamental and its higher harmonics. The results of the analysis gave the amplitude and phase associated with each term. Thus it was possible to assess the relative amplitudes of the higher harmonic terms. In general, for tidal currents in shallow Dampier Archipelago waters, the second and third harmonics were of comparable importance, one order of magnitude less in amplitude than the fundamental oscillation, and at least one order of magnitude greater than the amplitude of the fourth and all higher harmonics.

6.6.4 Tide-induced Residual Water Transport

The model results were used to calculate time-averaged volume transport vectors over the twelfth tide cycle at each grid cell. Within the Archipelago, the residual volume flux rate estimates due to the tidal dynamics alone were low. The Eulerian transport velocities (defined as the nett rate of volume flux per unit width divided by the mean depth of the water column) achieved a maximum of 5 cm s^{-1} to the SW in the coastal shallows of southern Mermaid Strait. The general level of transport velocities in the Archipelago was considerably lower than this, being typically 1 cm s^{-1}. The omission of the momentum advection terms from this model run is expected to have affected the estimation of the residual volume flux rates chiefly near narrow channels, sharply-curved headlands, and areas of shallow water. However, the conclusion that tide-induced residual movements are generally weak is not expected to change.

6.7 Comparison of Results from Model and Field Measurement

The semi-diurnal constituents of the field and model results were compared. Amplitude and phase values for the fundamental (semi-diurnal) mode of the model solution were derived at selected locations through the application of the Discrete Fourier Transform to the output time series of water levels and velocity components. Tidal analyses of tide gauge and current meter data gathered from the study area provided values for the amplitudes and phases of the major tidal constituents.

The locations of these oceanographic instruments are shown in Figure 3. Tide gauge 1 was deployed by R.K. Steedman and Associates for Woodside Offshore Petroleum Pty Ltd, and the 90 days' data analysed by Holloway (1983). Tide gauge 2 was deployed at Withnell Bay by the Public Works Department, WA, and 12 months' data analysed (G.W. Lennon, pers. comm.). The other instruments referred to were deployed for six weeks and analysed by the Department of Conservation and Environment.

For the semi-diurnal vertical tide, the cross-shelf amplification ratio and phase change predicted by the model (from outer model boundary grid cell (31,16) and model grid cell (4,14)) were found to be in good agreement with values derived from data collected at tide gauge 1 and tide gauge 2 (Figure 3). The results are given in Table 2.

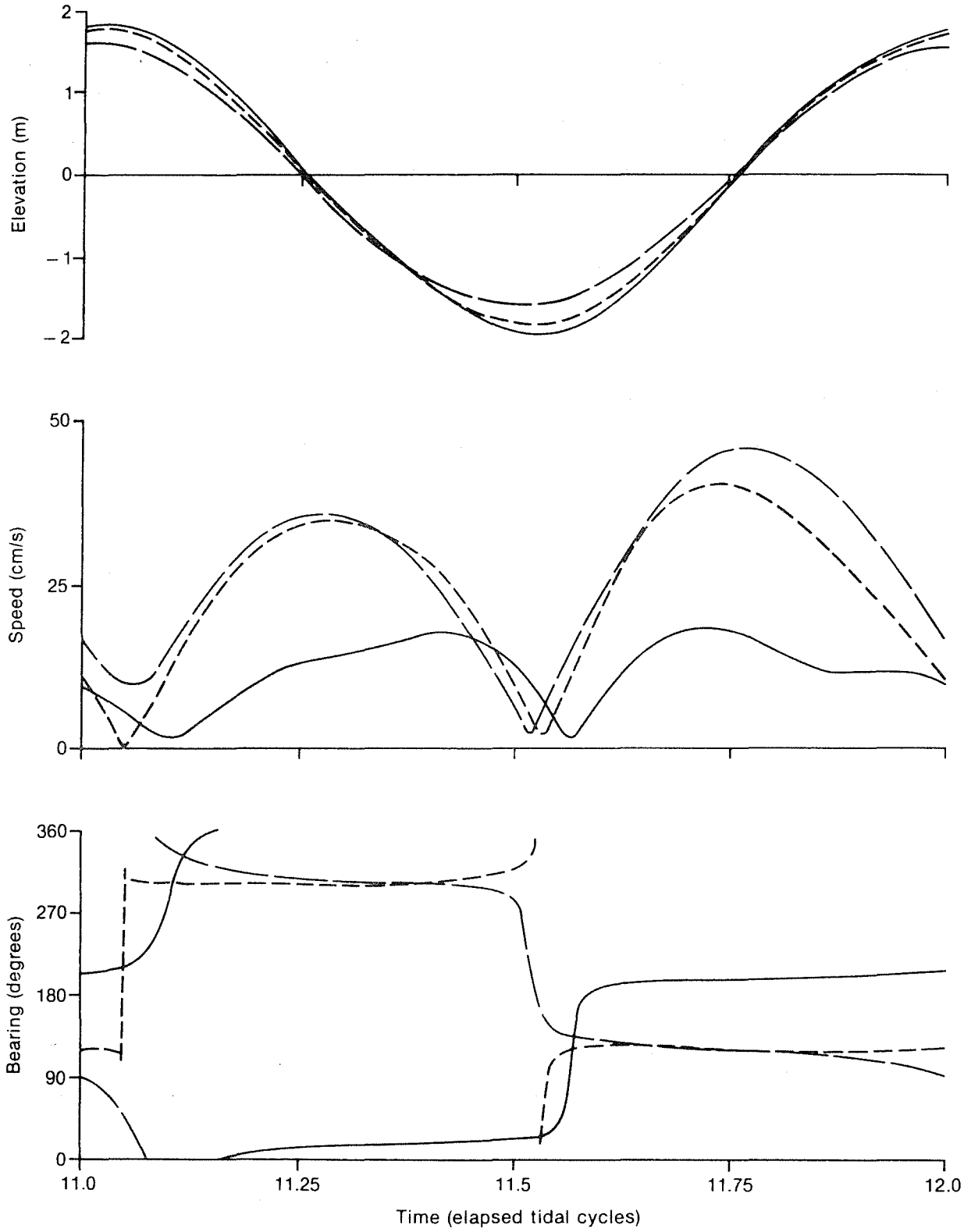

Figure 8(a) : A cross-shelf comparison of water level, current speed and direction time-series derived from model grid cells (4, 14) within Mermaid Sound (————), (10,13) at Mermaid Sound entrance (— — — —), and (27, 13) near the outer model boundary (—— ——).

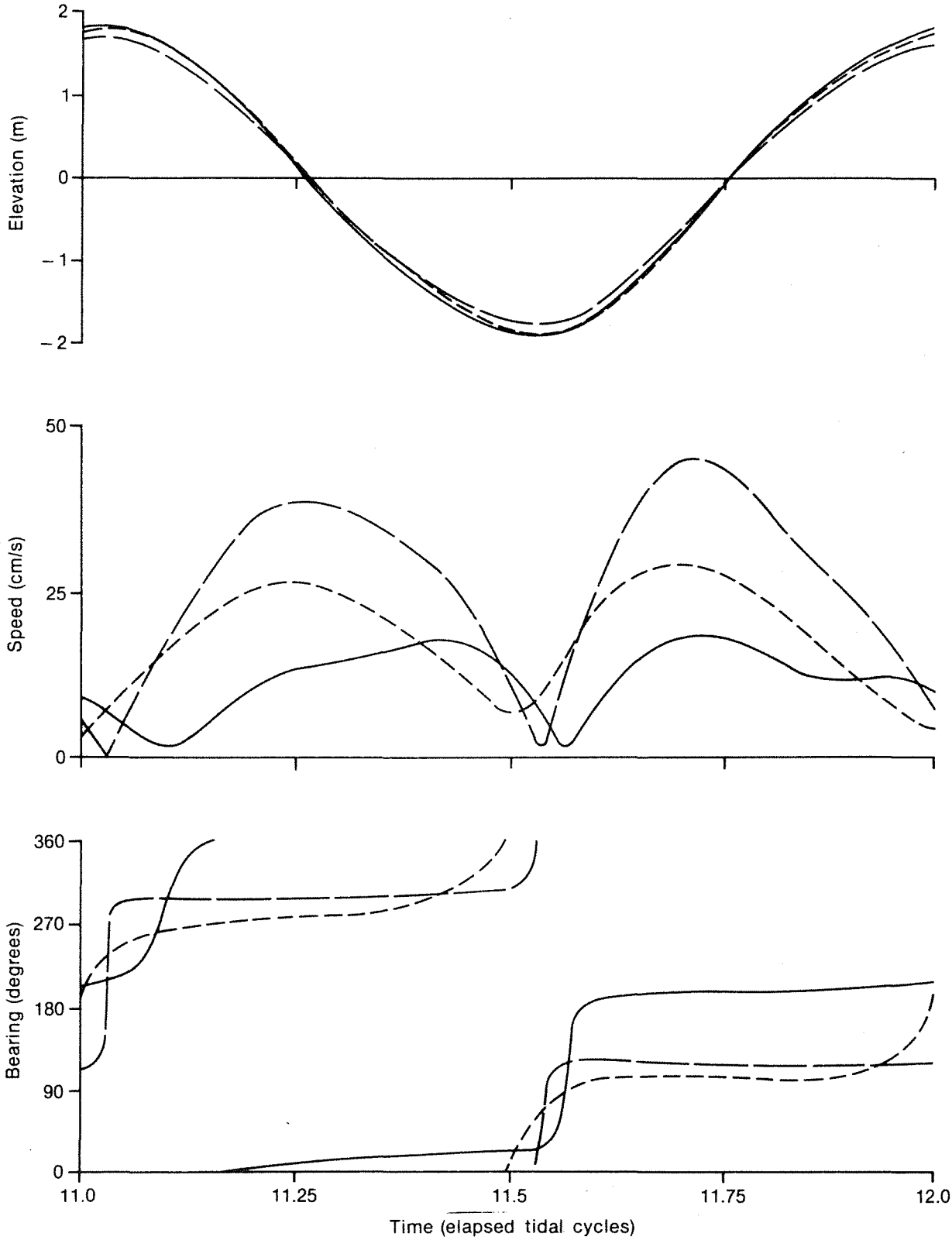

Figure 8(b) : A long-shelf comparison of water level, current speed and direction time-series derived from model grid cells (4, 14) within Mermaid Sound (————), (4, 21) within Mermaid Strait (— — — —), and (5, 29) south-west of Dampier Archipelago (—— ——).

TABLE 2

Comparison of measured and modelled tidal amplification and phase lag, cross-shelf

	Field Result	Model Result
Cross-shelf amplitude ratio	1.23	1.21
Cross-shelf phase variation (degrees)	6	5

In the long-shore direction, model results from grid cells (4,14) and (5,29), and analysed tidal constants from tide gauges 2 and 3 (Figure 3) exhibited similar ratios and almost zero phase difference. The results are shown in Table 3.

TABLE 3

Comparison of measured and modelled tidal amplification and phase lag, long-shore

	Field Result	Model Result
Long-shore amplitude ratio	0.95	0.91
Long-shore phase variation (degrees)	-1	0

The model is based on vertically-integrated equations and solves for the depth-averaged current velocities. Thus, before the model and field results for tidal currents can be properly compared, the effects of wind and other non-tidal influences must be removed from the current meter records, and some form of depth-averaging applied. This can be difficult in density stratified waters where the current response can vary with depth. Holloway (1983) did show however that the tidal currents of the inner and mid North-West Shelf are essentially barotropic, and the waters of the Dampier Archipelago are known to be generally well-mixed (D.C.E, unpublished data).

Tidal harmonic analyses were performed for each horizontal component of the data recorded by current meters located as shown in Figure 3. The tidal constants obtained were then used to calculate the properties of tidal current vector ellipses (see Godin 1972). These ellipses describe the time variations of tidal constituent current vectors at a particular site. They summarise maximum and minimum current speeds, directions of ebb and flood, phase, and sense of current vector rotation. A similar technique was applied to the Fourier transformed model velocity results. Table 4 presents a comparison of tidal current properties (derived from field and model). The maximum tidal current speeds quoted for the analysed current meter records are equivalent values for mean spring tides derived from the M2 constituent values.

TABLE 4

Comparison of modelled and measured tidal current ellipses

Location	Tidal Ellipse Properties			
	Max Speed (ms^{-1})	Phase (degrees)	Orientation (degrees N)	Sense of rotation
Current meter 5	0.14	-52	14	Clockwise
Grid cell (4,14)	0.16	-55	15	Clockwise
Current meter 7	0.42	-49	318	Clockwise
Grid cell (10,13)	0.35	-39	300	Clockwise
Current meter 4	0.26	-28	284	Clockwise
Grid cell (4,21)	0.25	-23	279	Clockwise
Current meter 6	0.41	-28	272	Anticlockwise
Grid cell (8,18)	0.47	-31	288	Anticlockwise

Agreement between modelled and measured tidal current ellipse attributes is good considering the qualifications mentioned above, the coarse resolution of the model, and the fact that there is not an exact correspondence between model output and field measurement locations. The maximum tidal speeds compare well. The phase relationships of the actual tidal currents are reproduced in the model; the semi-diurnal tidal currents of Mermaid Sound lag the shelf currents, and the currents in Mermaid Strait lead the shelf currents. Ellipse orientations (expressed as the bearing of the ebb current direction) are in good agreement within the Archipelago. On the open shelf, modelled ellipse orientations tend to align more cross-shelf with increasing distance offshore. This is consistent with the results obtained by Holloway (1983) from tidal analyses of offshore current meters. The sense of rotation of the tidal constituent current vectors is correctly reproduced. This is determined on the shelf by the action of the Coriolis force, but within the Archipelago it is conditioned by bathymetry.

6.8 Discussion

The nature of the force balance which governs the tidal motion was determined by calculating the magnitude of terms in the momentum equations at several points in the model and at several time instants.

On the open continental shelf the dynamic balance was found to be between the fluid acceleration and the pressure gradient driving force, caused by the slope of the water surface. Maximum acceleration occurs at times when the current is weak and reversing direction; at these times the Coriolis and bottom friction terms are at least an order of magnitude smaller than the pressure gradient force. At peak tidal speeds the Coriolis force and to a lesser extent the bottom friction dominate the temporarily weak, reversing pressure gradient force. Directed perpendicularly to the left of the current direction (southern hemisphere), the Coriolis force gives rise to an anti-clockwise sense of rotation of tidal currents on the shelf.

Within the Archipelago, in relatively shallow, confined waters, it was found that the principal force balance along the major current axes is between the fluid inertia (acceleration), the pressure gradient force, and the bottom

frictional stress. Strongest peak tidal currents occur in locations where large pressure gradients are able to be sustained. These locations occur toward the seaward entrances of the Archipelago. For example, Figures 6(b) and (c) indicate that between Enderby Island and Rosemary Island, seaward-directed water-surface slopes of at least 0.75×10^{-5} are sustained for more than a quarter of a tidal cycle. This gradient is first achieved due to the cross-shelf amplification of the tidal wave and is then sustained by the delay in the flooding or draining of the inshore waters.

The relatively rapid transition from peak ebb to peak flood currents in shallow water was also explained in dynamic terms. Significant deceleration of the ebb current is caused by a large opposing pressure gradient force and by a high level of frictional resistance. The effect of bottom stress is high for two reasons: water speed is initially high, and the height of the water column on which bottom stress operates becomes smaller as low water is approached. Once the current begins to flood, acceleration is again significant because of a large driving pressure gradient force and because the effect of frictional resistance is low, due initially to low velocities and subsequently to a high water level. Similar arguments may be used to explain the slower transition from peak flood to peak ebb currents.

The model was re-run with an increased value of the bottom friction coefficient ($k = 0.004$) and the results compared with those of the original model run ($k = 0.0025$). Water elevation showed small relative changes in amplitude (maximum 2%) and phase (up to 15 minutes). Changes in the tidal current response were more significant, with peak speeds changing by up to 10% and with their times of occurrence differing by up to 40 minutes. The greatest changes occurred in shallow water. Tidal residual volume flux rates through the Archipelago increased, even though the flux rates on the shelf decreased. These results provide further evidence of the role played by non-linear bottom friction in shallow water.

The model was also run with constant long-shelf tidal amplitude at the outer boundary. This was achieved by setting the value of l to zero in the open boundary conditions (10) and (11). The cross-shelf amplification of the vertical tide only slightly decreased (about 4%) and the phase change was not great. The most obvious changes occurred to the velocity field. The ebb and flood of water on the shelf was directed in an almost cross-shelf direction; peak speeds were reduced, and the tidal ellipses were less elongated. Within the Archipelago, peak current speeds changed by up to 20% and the timing of the peaks differed by up to two hours. This model simulation confirmed the role played by long-shelf tidal amplitude gradients in the generation of long-shelf components of the tidal current. It also served to illustrate the sensitivity of the model solution to changes in the boundary conditions. It is concluded that the details of tidal flow patterns within the Archipelago are dependent not only on the form of the local water body and the relative importance of processes operating locally in shallow water, but also on the regional long-shelf gradient of tidal amplitude, arising as a function of oceanic forcing and the regional form of the continental shelf.

The non-linear momentum advection terms were included in a trial model run using a slightly more simplified 'Dampier Archipelago' layout (channels were enlarged to two grid cells in width). A stable, convergent model solution was obtained. The fully non-linear model is therefore considered operational. The results suggest that the major influence of the momentum advection terms is restricted to areas where current speeds are high and non-uniform, e.g. near channels, well-defined promontories or headlands.

In several studies (e.g. Flather 1976, Fandry 1981) it has been shown that certain combinations of open boundary conditions may cause grid scale oscillations in the elevation field and unrealistically large or incoherent currents, which first appear near to the open boundaries. The use of open boundary conditions as described in section 6.4 does not seem to have been documented elsewhere in the literature. A feature of the results obtained and presented above is the stability and smoothness of the elevation and velocity fields, particularly near the open boundaries. This may be attributed to the following factors:

- the condition applied along the outer long-shelf boundary also satisfies the conditions imposed at the cross-shelf boundaries, so that there is no incompatibility at the corners of the modelled region where open boundaries meet

- the cross-shelf boundary conditions do not impose prior information concerning cross-shelf variations of water level or currents.

These boundary conditions could be applied to simulations of either the M2, the S2, or the sum of these semi-diurnal tidal components. However alternative conditions would be required to simulate combinations of semi-diurnal and diurnal components for which the long-shelf tidal amplitude gradients differ.

7. SUMMARY

A two-dimensional, vertically-integrated, numerical, hydrodynamic model has been developed to facilitate the better understanding of current flow and water level regimes on continental shelves, nearshore waters, coastal inlets and embayments of interest to the Department of Conservation and Environment. The model can simulate the major types of water flow found in Western Australian coastal waters, ranging from predominantly tidal, such as occurs off the Kimberley coast, to predominantly wind-driven, such as occurs off the south and south-west coasts. The interaction of regional scale, continental shelf currents with local coastlines and bathymetry may also be investigated with appropriately set boundary conditions.

Based on equations of mass and momentum conservation, the model calculates finite-difference solutions describing the spatial distribution and evolution of water levels and depth-averaged horizontal currents in water bodies of specified coastal form and bathymetry. The model includes the dynamics associated with sea surface slopes, applied wind stress, bottom friction, the effects of the earth's rotation, and the advection of momentum. An initial field of motion must be specified, and water level or current data must be supplied at the open (sea) boundaries throughout the course of the model run. Realistic simulations of natural coastal water movements rely heavily on the accuracy of the open boundary data input to the model.

The model was first applied to an investigation of the tides and tidal streams of the Dampier Archipelago and inner North-West Shelf, using a spatial resolution of 3 km. This investigation has confirmed that, for the dominant semi-diurnal tide, the regional long-shelf gradient of tidal amplitude is primarily responsible for driving the long-shelf component of tidal currents on the shelf, as suggested by Holloway (1983). Furthermore, the model has shown that the strength and direction of tidal currents within the Archipelago are strongly governed by the value of this gradient. This important regional feature has been included in the formulation of the open boundary conditions. At the outer, long-shelf model boundary, values of water level have been

prescribed as time-dependent sinusoids with amplitude varying exponentially as a function of location along the boundary. At the cross-shelf open boundaries the long-shelf gradient of tidal amplitude has again been used, this time in the form of a relationship between the normal derivative of water level and the water level itself. Thus no prior information concerning cross-shelf structure has been supplied to the model. The solution resulting from this set of boundary conditions, not documented elsewhere, shows excellent stability and smoothness near the open boundaries.

The results obtained from the model compare favourably with the tide gauge and current meter records collected in the study area. The increase in amplitude and the phase lag of the vertical tide in the cross-shelf (shoreward) direction have been correctly simulated. Properties of the tidal streams (speed and direction of peak current vectors, phase relationships, sense of rotation of the currents) have been substantially reproduced by the model, both on the open shelf and within the Archipelago. In deep water, on the open continental shelf, the essential nature of the motion is governed by a balance between fluid acceleration and pressure gradient force; the bottom friction is dynamically unimportant. Thus the peak currents occur at times of small water level gradient. In shallow water the force balance is more complex, involving the fluid acceleration, the pressure gradient force and the bottom friction. Peak currents occur at times and in places of sustained sea surface gradients. Generally, the strongest tidal currents occur near the outer extremities of the Archipelago, particularly in the natural channels passing immediately off the SW end of Enderby Island, and between Enderby and Rosemary Islands; however, peak simulated tidal current speeds in the Mermaid Sound entrance diminish to the north-west. The tidal current regime is generally weak in the innermost reaches of the Archipelago, except in some of the interisland passages. Currents in Mermaid Sound lag shelf currents, whereas currents in Mermaid Strait lead shelf currents. The current variations become progressively more asymmetrical in shallow water locations. Residual (time-averaged) volume flux rates due to tidal dynamics alone are low.

Presently the model is being used to examine the relative contributions of tidal, wind-driven and regional currents to the flushing and water exchange of the Dampier Archipelago. Based on an examination of wind and tidal data, a set of representative case studies is being prepared. These will be used to force the model. The results of these simulations will provide information on the range of flushing rates experienced in the study area.

8. FUTURE DIRECTIONS

In nearshore, flat, shallow margins, changes in water level can cause the shoreline to advance or recede over significant distances horizontally. Successive inundation and exposure of isolated shoal banks can cause redirection of currents, the flow being confined to deeper channels at low water and flowing more diffusely across the banks at high water. It is planned to cater for flooding and drying banks in the model through the use of moveable boundaries.

The transport, fate and residence times of materials released into a water body from point or diffuse sources depends on details of flow variations in time and space, dispersion processes, and the decay or transformation rates of the materials. It is planned to extend the model program to compute trajectories of "particles" released into the modelled flow field at known times and places. The effects of dispersion and non-conservative processes will also be included. This capability will be used to assess zones of pollution about sources of effluent discharge, and to determine residence time and water exchange regimes in estuaries or embayments.

9. ACKNOWLEDGEMENTS

The author thanks Mr D. Pitt for writing the computer plotting programs. The tidal analyses of current meter data were performed using computer programs documented in Barnes and Holloway (1982). Dr P. Holloway and Dr P. Craig of the Centre for Environmental Fluid Dynamics, University of Western Australia, kindly read and commented on the manuscript.

10. REFERENCES

Arakawa A. (1972) Design of the UCLA general circulation model. Numerical Simulation of Weather and Climate, Tech. Rep. 7, Dept, Meteorol. Univ. Calif. L.A.

Barnes I. & Holloway P. (1982) A system of computer programs for the analysis of oceanographic data time series. Environ. Dyn. Rept. ED-82-018, Dept. Civ. Eng., Univ. West. Aust.

Bode L., Mason L.B., Sobey, R.J. & Stark K.P. (1981) Hydrodynamic studies of water movements within the Great Barrier Reef region. (i) Preliminary investigations. Res. Bull. CS27, Dept. Civ. & Sys. Eng., James Cook Univ.

Cheng R.T., Powell T.M. & Dillon T.M. (1976) Numerical models of wind-driven circulation in lakes. Appl. Math. Model. I, 141-159

Courant R., Friedrichs K. & Lewy H. (1928) Uber die partiellen Differenzengleichungen der mathematishchen. Phys. Math. Ann., 100, 32-74

Csanady G.T. (1982) 'Circulation in the coastal ocean.' pp 174-176, (D. Riedel: Dordrecht)

Easton A.K. (1970) The tides of the continent of Australia. Res. Paper 37, Horace Lamb Centre, Flinders Univ. S. Aust.

Fandry C.B. (1981) Development of a numerical model of tidal and wind driven circulation in Bass Strait. Aust. J. Mar. Freshw. Res. 32, 9-29

Flather R.A. & Heaps N.S. (1975) Tidal computations for Morecambe Bay Geophys. J.R. Astr. Soc. 42, 489-517

Flather R.A. (1976) A tidal model of the north-west European continental shelf. Mem. Soc. R. Sci. Liege, 6 series, 10, 141-164

Garrett C. (1975) Tides in gulf. Deep-Sea Res. 22, 23-35

Godin G. (1972) 'The analysis of tides.' (Liverpool University Press: Liverpool)

Hicks B.B. (1972) Some evaluations of drag and bulk transfer coefficients over water bodies of different sizes. Boundary-layer Meteorol. 3, 201-213

Holloway P.E. (1982) Internal tides on the Australian North-West Shelf: a preliminary investigation. Environ. Dyn. Rept. ED-82-022, Dept. Civ. Eng., Univ. West Aust.

Holloway P.E. (1983) Tides on the Australian North-West Shelf. Aust. J. Mar. Freshw. Res. 34, 213-230

Howarth M.J. & Pugh D.T. (1983) Observations of tides over the continental shelf of North-West Europe. In 'Physical oceanography of coastal and shelf seas.' (ed. B. Johns) pp 135-186 (Elsevier: Amsterdam)

Hunter J.R. (1982) User's manual for two-dimensional numerical hydrodynamic model (programs M2D104, M2D125 and MCD103). Report U80-50, Unit for Coastal and Estuarine Studies, Marine Science Laboratories, Menai Bridge, Anglesey

Lamb H. (1932) 'Hydrodynamics' (6th ed.), (Cambridge University Press: Cambridge)

Pingree R.D. & Maddock L (1977) Tidal residuals in the English Channel J. Mar. Biol. Assoc. U.K. 57, 339-354

Pingree R.D. & Maddock L. (1978) The M4 tide in the English Channel derived from a non-linear numerical model of the M2 tide. Deep-Sea Res. 25, 53-63

Roberts K.V. & Weiss N.O. (1966) Convective-difference schemes, Math. Comput. 20, 272-299

Schwiderski E.W. (1979) Global ocean tides, part 2: The semi-diurnal principal lunar tide (M2), atlas of tidal charts and maps. Naval Surface Weapons Centre, K05 Dahlgren, Virginia, Rep. NSWC TR 79-414

Zimmerman J.T.F. (1978) Topographic generation of residual circulation by oscillatory (tidal) currents. Geophys. Astrophys. Fluid Dyn. 11,35-47